The Astrophysical Journal, 985:126 (12pp), 2025 May 20 https://doi.org/10.3847/1538-4357/adc722

Temporarily Quiescent Galaxies at Cosmic Dawn: Probing Bursty Star Formation

Viola Gelli[1,2], Andrea Pallottini[3,4], Stefania Salvadori[5,6], Andrea Ferrara[4], Charlotte Mason[1,2], Stefano Carniani[4], and Michele Ginolfi[5,6]
[1] Cosmic Dawn Center (DAWN), Denmark; viola.gelli@nbi.ku.dk
[2] Niels Bohr Institute, University of Copenhagen, Jagtvej 128, 2200 København N, Denmark
[3] Dipartimento di Fisica "Enrico Fermi," Universitá di Pisa, Largo Bruno Pontecorvo 3, Pisa I-56127, Italy
[4] Scuola Normale Superiore, Piazza dei Cavalieri 7, I-56126 Pisa, Italy
[5] Dipartimento di Fisica e Astronomia, Universitá degli Studi di Firenze, via G. Sansone 1, 50019, Sesto Fiorentino, Italy
[6] INAF/Osservatorio Astrofisico di Arcetri, Largo E. Fermi 5, I-50125, Firenze, Italy
Received 2025 January 27; revised 2025 March 27; accepted 2025 March 28; published 2025 May 19

Abstract

The bursty, time-variable nature of star formation in the first billion years, as revealed by JWST, drives phases of *temporary quiescence* in low-mass galaxies that quench after starbursts. These galaxies provide unique probes of the burstiness of early star formation and its underlying physical processes. Using the SERRA cosmological zoom-in simulations, we analyze over 200 galaxies with $M_\star < 10^{9.5} M_\odot$ at $z \sim 6$–8, finding that most experience quiescent phases driven by stellar feedback, with minimal influence from environmental effects. The fraction of temporarily quiescent galaxies increases with decreasing mass and luminosity, representing the dominant population at $M_\star < 10^8 M_\odot$ and $M_{\rm UV} > -17$. By forward modeling their spectral energy distributions, we show that they are faint ($\langle M_{\rm UV} \rangle = -15.6$ for $M_\star = 10^8 M_\odot$), have strong Balmer breaks (>0.5), and no emission lines. Comparing our predicted fractions with JWST results, we find similar luminosity-dependent trends; however, the observed fractions of temporarily quiescent galaxies at $M_{\rm UV} \sim -20$ to -19 are higher, suggesting that stronger feedback or additional mechanisms beyond supernovae may be at play. We propose searching for F200W dropouts and satellites in the proximity (<5″) of massive ($>10^{10} M_\odot$) galaxies as effective strategies to uncover the hidden majority of faint ($M_{\rm UV} > -17$), temporarily quiescent systems, crucial for constraining early feedback processes in low-mass galaxies.

Unified Astronomy Thesaurus concepts: High-redshift galaxies (734); Cosmology (343); Galaxy evolution (594); Dwarf galaxies (416)

1. Introduction

With its unprecedented depth and sensitivity, the James Webb Space Telescope (JWST) is enabling us to study the star formation histories (SFHs) of galaxies in the first billion years of the Universe in remarkable detail. The way galaxies form their stars over time is determined by the complex interplay of gas cooling, accretion, feedback processes, and environmental factors. Low-mass galaxies, with their shallow gravitational wells, are especially sensitive to these effects, leading to stochastic, or "bursty," SFHs characterized by strong fluctuations over short timescales (e.g., S. R. Furlanetto & J. Mirocha 2022; K. G. Iyer et al. 2024). During the first billion years since the Big Bang, the Universe is largely dominated by such low-mass galaxies, and bursty star formation is predicted to be common, as shown by several cosmological simulations (e.g., X. Ma et al. 2018; A. Pallottini et al. 2022; G. Sun et al. 2023a; A. Bhagwat et al. 2024).

Constraining the level of "burstiness" in high-z galaxies is important for several reasons. First, understanding the time variability of the SFHs is key for unveiling the physics regulating it, as different feedback and accretion processes act on different timescales (e.g., K. G. Iyer et al. 2020; S. Tacchella et al. 2020). Second, bursty star formation can have significant implications on multiple observables: the UV luminosity functions (C. A. Mason et al. 2023; J. Mirocha & S. R. Furlanetto 2023; A. Pallottini & A. Ferrara 2023; X. Shen et al. 2023; G. Sun et al. 2023b; V. Gelli et al. 2024a; A. Kravtsov & V. Belokurov 2024), the ionizing photon budget (I. Nikolić et al. 2024), the mass–metallicity relation (A. Pallottini et al. 2024), and even the potential detectability of Population III galaxies (H. Katz et al. 2023).

JWST results are indeed providing increasing evidence of bursty star formation in the Epoch of Reionization (EoR). Galaxies at fixed stellar mass or luminosity exhibit large scatter in the distributions of properties, such as the star formation rate (SFR; e.g., L. Ciesla et al. 2024, J. W. Cole et al. 2025), the gas metallicity (e.g., K. E. Heintz et al. 2023; T. Morishita et al. 2024), stellar ages (e.g., L. Whitler et al. 2023), emission line strengths (e.g., R. Navarro-Carrera et al. 2024), and ionizing photon production efficiencies (e.g., R. Endsley et al. 2024b; G. Prieto-Lyon et al. 2023; R. Begley et al. 2025).

A key implication of bursty star formation is the possibility that galaxies may be quenched following strong starbursts, resulting in a population of *temporarily quiescent* high-z galaxies[7] (e.g., V. Gelli et al. 2020; A. L. Faisst & T. Morishita 2024). JWST has indeed also provided the very first detections of low-mass post-starburst quiescent galaxies in the EoR (V. Strait et al. 2023; T. J. Looser et al. 2024; W. M. Baker et al. 2025). The mechanisms driving this quenching are still debated: supernova (SN) feedback alone seems insufficient to abruptly suppress star formation in the short timescales observed (V. Gelli et al. 2023; T. Dome et al. 2024; V. Gelli

[7] To describe this particular class of galaxies, different definitions have been adopted: "mini-quenched," "smoldering," "napping," "lulling," etc. In this paper, we refer to them as "temporarily quiescent" galaxies.

et al. 2024b), and the environment may also play a role in some cases (e.g., Y. Asada et al. 2024).

Reconstructing and interpreting the evolution of individual galaxies is challenging, as recent starbursts outshine older stellar populations (e.g., C. Giménez-Arteaga et al. 2024; D. Narayanan et al. 2024) and a lack of emission lines can be confused with high escape fractions (e.g., M. W. Topping et al. 2022). To overcome these issues, we can use a statistical approach. Exploiting large samples of high-z galaxies, we can probe systems that are experiencing different stages of their star formation. By looking at these galaxies as an "ensemble" and quantifying the fraction of quiescent versus starbursting systems, we can gain insight into early galaxy formation.

In particular, the fraction of galaxies undergoing temporary quiescence is directly tied to the overall duration of these phases, encapsulating key information about the duty cycles and timescales of SFH variability. Observations of large samples of this new class of temporarily quiescent galaxies uncovered by JWST offer a unique way to probe bursty star formation and high-z quenching mechanisms.

Recently, several efforts have been made toward the identification of galaxies experiencing temporarily quiescent phases of star formation (T. J. Looser et al. 2023; R. Endsley et al. 2024a; J. Trussler et al. 2025), finding that they constitute a considerable fraction of the high-z low-mass and low-luminosity galaxy population. However, the physical interpretation of these results and comparison with theoretical models and simulations is complex and challenging, as observational samples are not complete in stellar mass and naturally biased toward the brighter and more luminous starburst phases of star formation (e.g., C. A. Mason et al. 2023; G. Sun et al. 2023a).

JWST is, however, finally enabling us to explore a broader range of SFRs of galaxies at $z > 6$, capturing not only the starbursts but also the fainter phases of the galaxies' highly time-variable SFHs.

In this paper, we use results from the SERRA cosmological simulations (A. Pallottini et al. 2022) combined with accurate forward modeling of galaxy spectra (V. Gelli et al. 2021) to predict the expected abundances of observable temporarily quiescent galaxies at high z. By comparing these predictions with recent JWST results, we aim to constrain the burstiness of galaxies in the EoR and infer the physical processes shaping it.

2. Methods

2.1. SERRA Cosmological Simulations

SERRA (A. Pallottini et al. 2022) is a suite of cosmological zoom-in simulations that follow the evolution of typical Lyman break galaxies ($M_\star \simeq 10^{10} M_\odot$) and their environments in the EoR. MUSIC (O. Hahn & T. Abel 2011) is adopted to generate initial conditions at $z = 100$ in a cosmological volume of $(20\,\mathrm{Mpc}/h)^3$ by assuming a Planck Collaboration et al. (2014) cosmology.[8] RAMSES (R. Teyssier 2002) is used to follow the evolution of dark matter, stars, and gas by adopting baryon mass resolution of $1.2 \times 10^4 M_\odot$ and spatial resolution of $\simeq$20 pc in the zoom-in regions, i.e., about the mass and size of molecular clouds. SERRA allows for on-the-fly radiative transfer via RAMSES-RT (J. Rosdahl et al. 2013) that is coupled (A. Pallottini et al. 2019) with the photon–gas interactions handled with KROME (T. Grassi et al. 2014), by solving for the nonequilibrium chemical network up to molecular hydrogen (H_2) formation (A. Pallottini et al. 2017a).

Stars form following a M. Schmidt (1959)–R. C. Kennicutt (1998) relation depending on the H_2 density, and assuming a P. Kroupa (2001) initial mass function. Stellar feedback modeling includes SNe explosions, winds, and an approximate treatment of radiation pressure (A. Pallottini et al. 2017b). STARBURST99(C. Leitherer et al. 1999) is used to account for the mechanical energy injection (SN and winds), photon inputs, and chemical yields, depending on the stellar age and metallicity, that are taken from PADOVA stellar tracks (G. Bertelli et al. 1994), covering a metallicity range of $Z_\star/Z_\odot = 0.02$–1.0. As a $1.2 \times 10^4 M_\odot$ resolution does not allow for following the evolution of the first stars and minihalos, their effect is accounted for by setting the initial gas metallicity to a floor value of $Z_{\rm floor} = 10^{-3} Z_\odot$ (J. H. Wise et al. 2012; A. Pallottini et al. 2014).

In this work, we analyze multiple SERRA galaxies taken in the $6 < z < 8$ redshift range. To quantify the importance of environmental effects on the evolution of low-mass galaxies, we select and analyze both *central* galaxies and *satellite* galaxies orbiting more massive systems. However, the typical clustering algorithm for galaxy identification (e.g., S. R. Knollmann & A. Knebe 2009; P. S. Behroozi et al. 2013) is calibrated for large cosmological simulations and can experience problems in pinpointing the satellites located in the highest-density regions, particularly in the case of zoom-in simulations. Thus, first we use ROCKSTAR (P. S. Behroozi et al. 2013) to select galaxies $M_\star < 10^{10.5} M_\odot$ and then the low-mass satellites sample is extracted using a stellar-density-based method (V. Gelli et al. 2020), checking a posteriori for the presence of a dark matter (sub)halo.

The sample used in this paper consists of 78 central and 131 satellite galaxies at $6 < z < 8$ with stellar masses in the range $M_\star = 10^7$–$10^{9.5} M_\odot$.

2.2. Spectral Energy Distribution Modeling

To produce synthetic spectral energy distributions (SEDs) of the simulated galaxies, first, we model the stellar emission using STARBURST99 (C. Leitherer et al. 1999), ensuring consistency with the simulation prescriptions. In particular, we compute the emission from each stellar particle based on its individual age and metallicity, then sum their contributions to obtain the total galaxy spectrum.

CLOUDY (G. J. Ferland et al. 2017) is used to compute nebular line emission from the galaxies' interstellar medium, taking the gas density, metallicity, turbulent structure, and radiation field into account (L. Vallini et al. 2018; A. Pallottini et al. 2019). We compute the main lines typically contributing to the rest-frame UV–optical spectrum (i.e., hydrogen Hα, Hβ, Hγ, oxygen [O II] $\lambda\lambda$3726,3729 and [O II]$\lambda\lambda$4959,5007, and carbon (C III]1909) by summing cell-by-cell luminosities from CLOUDY and assuming a Gaussian profile with a width determined by the thermal and turbulent motions (see M. Kohandel et al. 2020).

Finally, we take the presence of dust in the galaxies into account, which can attenuate the intrinsic spectrum (i.e., see V. Gelli et al. 2021). In particular, we adopt a dust-to-metal ratio of $f_d = 0.08$ and assume MW-like dust (C. Behrens et al. 2018): we use the extinction curve from J. C. Weingartner & B. T. Draine (2001) to attenuate the synthetic intrinsic SED of

[8] Throughout the paper, we assume a ΛCDM model with vacuum, matter, and baryon densities in units of the critical density $\Omega_\Lambda = 0.692$, $\Omega_m = 0.308$, $\Omega_b = 0.0481$, Hubble constant $H_0 = 67.8\,\mathrm{km\,s^{-1}\,Mpc^{-1}}$, spectral index $n = 0.967$, and $\sigma_8 = 0.826$.

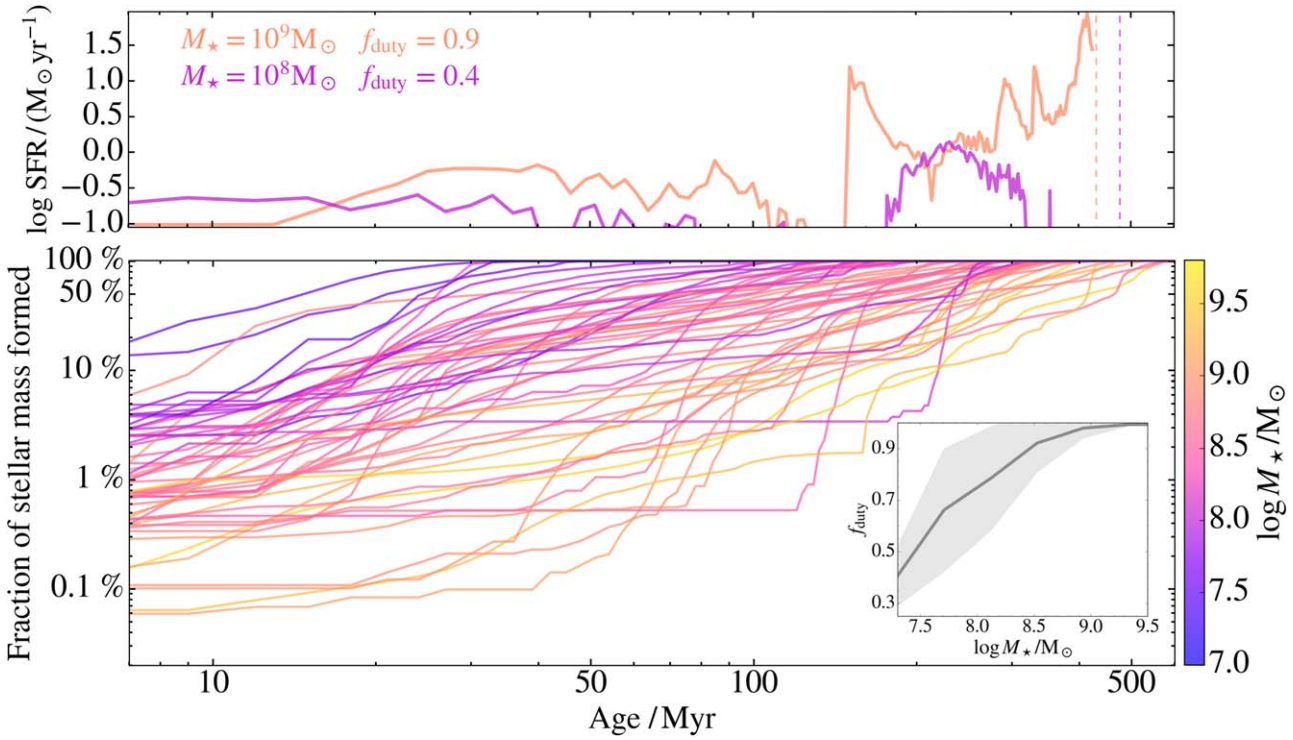

Figure 1. The top panel shows the SFH of two typical galaxies, one with high mass and high duty cycle, the other with low mass and low duty cycle, and undergoing a quiescent phase at the end of the simulation ($z \sim 6$, indicated by the dashed vertical line). The bottom panel shows the fraction of stellar mass formed with respect to the final stellar mass ($M_\star$) of each galaxy as a function of the time elapsed from its first star formation event. The colors indicate the final stellar mass of the galaxies. Most galaxies experience periods of quiescence during their early evolutionary stages. The inset shows the mean trend of the duty cycle, i.e., the fraction of time spent in activity, that increases as a function of the stellar mass.

each galaxy.[9] Note that the assumptions for dust differ from V. Gelli et al. (2021), where an SMC-like extinction curve and $f_d = 0.3$ is adopted. This change of assumptions is driven by more recent ALMA measurements of high-z galaxies (R. J. Bouwens et al. 2022), which support a MW-like dust (A. Ferrara et al. 2022) and lower dust-to-metal ratios (N. Laporte et al. 2017; C. Behrens et al. 2018). However, the choice of different dust attenuation curves has minimal impact on the SEDs of the sources analyzed in this work due to the gas- and dust-poor nature of low-mass, temporarily quiescent galaxies.

3. The Physics of Bursty Galaxies

We here present the simulations' results for the sample of $6 < z < 8$, $M_\star < 10^{9.5} M_\odot$ galaxies, analyzing their bursty evolution and its impact on the SFR–$M_\star$ relation and on the fraction of temporarily quiescent galaxies.

3.1. Stellar Mass Buildup

To understand how galaxies form and evolve in the simulations, in the main panel of Figure 1, we show the fraction of stellar mass formed as a function of the time elapsed from the first star formation event in the galaxy. The colors correspond to the final stellar mass $M_\star$ of each galaxy. Low-mass systems ($M_\star < 10^8 M_\odot$) preferentially form all their stars in a few tens of Myr, whereas the stellar mass buildup is much longer (up to ∼500 Myr) in more massive systems.

The rise in the mass of the galaxies is not always regular and smooth. Rather, most SFHs are characterized by both rapid rises due to starburst events and prolonged phases in which the galaxies are rendered *temporarily quiescent* by feedback processes (horizontal tracks).

Most galaxies, even those with a final mass $M_\star > 10^9 M_\odot$, experience periods of quiescence during the early stages of their evolution, typically within the first $\lesssim$200 Myr of their lifetimes, when they are less massive, i.e., when $M_\star \lesssim 10\%$ of their final stellar mass. Lower-mass systems are, in fact, more sensitive to feedback and more easily quenched, being less efficient in retaining gas in their shallow potential wells after H_2 photoevaporation and SN explosions.

The time variability of galaxies alternating between starbursting and quiescent phases can be quantified through their duty cycle, $f_{\rm duty}$, defined as the ratio of time spent in activity (SFR > 0) and the overall time since the formation of the galaxy (see Equation (1) in V. Gelli et al. 2023). As shown in the inset, the average duty cycle increases with the stellar mass, indicating that it is more likely for lower-mass galaxies to undergo a period of temporary quiescence.

In the top panel, we show as an example the SFH of two typical galaxies of different masses, highlighting their bursty time-variable evolution. The higher-mass galaxy undergoes a phase of temporary quiescence after its first main burst of star formation. As it builds up its mass, its average star formation rate increases. While its evolution remains bursty, marked by peaks and downturns, the galaxy becomes more stable against feedback processes, preventing further quiescent phases. The lower-mass system is quiescent by the end of the simulation

[9] As a test of the method, the continuum spectra of galaxies at $z = 7.7$ in the present sample have been compared with the SEDs resulting from 3D continuum radiative transfer post-processing done via SKIRT (M. Baes & P. Camps 2015) with the setup adopted in A. Pallottini et al. (2022). The SEDs obtained with the two methods are consistent.

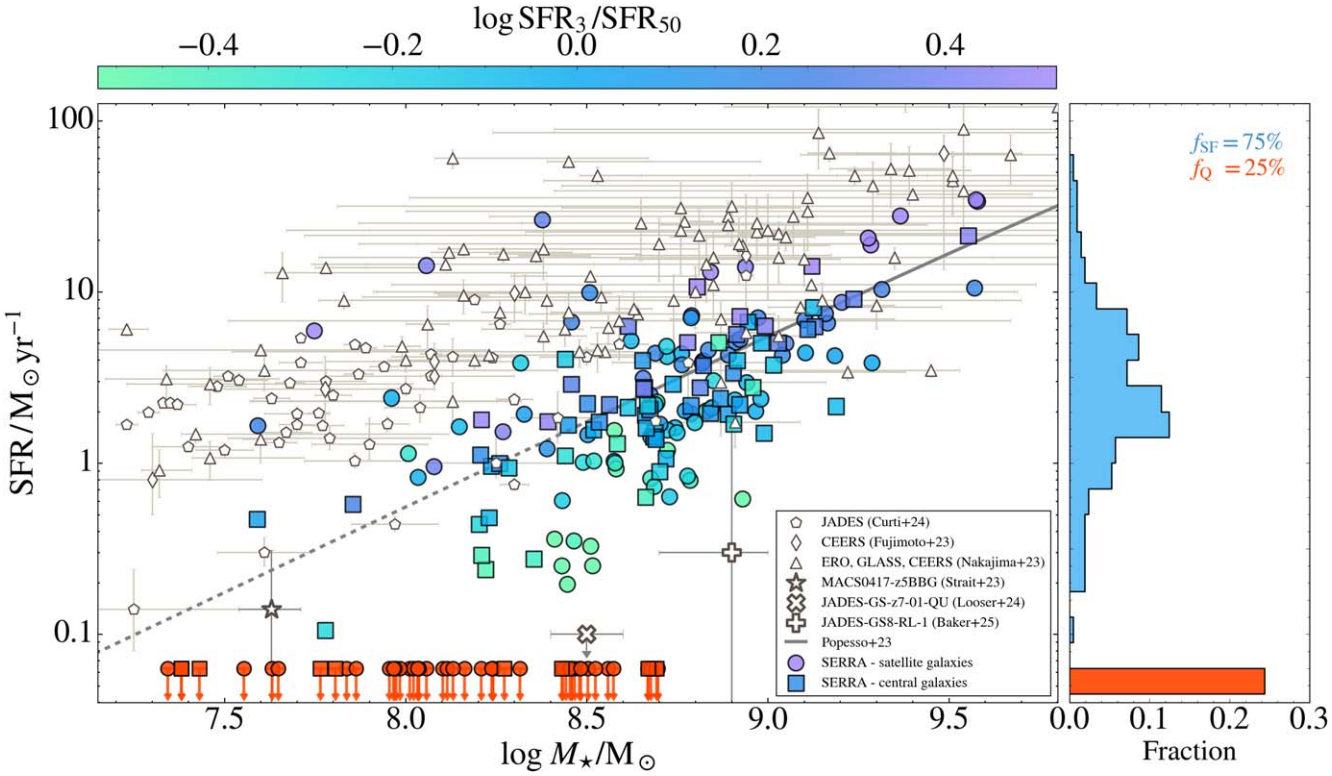

Figure 2. Stellar mass ($M_\star$)—SFR, averaged over 3 Myr, relation for a sample of 208 galaxies at $z = 6$–8 from the SERRA simulations (A. Pallottini et al. 2022). The galaxies are color coded with the ratio between SFR averaged over 3 Myr (SFR_3) and 50 Myr (SFR_{50}), which is an indicator of whether the galaxies are experiencing bursts (>1) or downturns (<1) of star formation. Galaxies undergoing phases of quiescence are shown in orange. Different markers distinguish satellite galaxies orbiting more massive companions (squares, 131) from central galaxies (circles, 78). We also show JWST results of $z \sim 4$–9 galaxies spectra from M. Curti et al. (2024), K. Nakajima et al. (2023), S. Fujimoto et al. (2023), T. J. Looser et al. (2024), V. Strait et al. (2023), W. M. Baker et al. (2025) and the $z \sim 6$ star-forming main sequence parameterization by P. Popesso et al. (2023), showing that JWST observations seem biased toward starbursting and high-SFR systems.

($z \sim 6$, marked by the dashed vertical line). Its previous evolution is similar to the first phases of the more massive galaxy, indicating that it may resume star formation again later on.

As we detect galaxies at specific times during their evolution, we want to study how their burstiness is expected to affect the observed SFR–$M_\star$ relation.

3.2. SFR–Stellar Mass Relation

In Figure 2, we show the SFR–$M_\star$ relation for the entire sample of $M_\star \lesssim 10^{9.5} M_\odot$ galaxies at $z \sim 6$–8. Their SFRs are in the range $\mathrm{SFR} = 0$–$50 M_\odot\ \mathrm{yr}^{-1}$, the average increasing with stellar mass, with the relation being characterized by a significant scatter, especially toward lower masses. This scatter is the direct result of the bursty evolution that galaxies experience in their lifetimes, characterized by peaks of SFR (up to $\sim 20 M_\odot\ \mathrm{yr}^{-1}$ for galaxies with $M_\star \sim 10^8 M_\odot$) and downturns in which the star formation is suppressed and can render some of them temporarily quiescent (SFR = 0, shown in orange). To quantify the burstiness phase that each galaxy is experiencing, we color code them according to the ratio between the instantaneous SFR_3, averaged over the last 3 Myr, and SFR_{50}, averaged over the last 50 Myr, similarly[10] to R. Endsley et al. (2024a). When $SFR_3/SFR_{50} > 1$, the galaxy is undergoing a starbursting phase, while when the ratio is <1, the system is experiencing a downturn in star formation.

At fixed stellar mass, galaxies with higher SFR values are typically in starburst phases, reaching $SFR_3/SFR_{50} \sim 5$, whereas galaxies with lower SFR are more likely to be experiencing downturns in star formation. Among these downturn galaxies, we note that only those with $M\star < 10^9 M_\odot$ experience strong suppression of star formation and can also undergo temporarily quiescent states. This is a direct consequence of how burstiness affects galaxies at different masses, with low-mass galaxies more susceptible to feedback.

The histogram in the right-hand panel displays the wide range of SFR covered by our sample of $M_\star = 10^7$–$10^{9.5} M_\odot$ galaxies. Interestingly, we see that systems undergoing a temporarily quiescent phase constitute a significant fraction of $z \sim 6$–8 galaxies, representing the $f_Q = 25\%$ of the population.

To assess the potential impact of different environments on the bursty evolution of high-z galaxies, in Figure 2, we distinguish central galaxies from satellite galaxies living in close proximity to a more massive galaxy. Comparing their distribution in the SFR–$M_\star$ relation, we find no large differences, with both types of galaxies roughly covering the same ranges of $M_\star$ and SFR. In regions of high star formation ($\mathrm{SFR} > 10 M_\odot \mathrm{yr}^{-1}$), satellites are more prevalent, but this is a statistical effect, as they constitute the majority of the sample (131 satellites to 78 central). However, when comparing the fraction of temporarily quiescent galaxies in the two subsamples, we find that for satellites the fraction is $f_{Q,\mathrm{sat}} = 32\%$, and for central systems it is $f_{Q,\mathrm{isol}} = 13\%$. As shown

[10] While different definitions of burstiness can be adopted (J. Leja et al. 2019; J. Chaves-Montero & A. Hearin 2021; A. Pallottini & A. Ferrara 2023; D. Langeroodi & J. Hjorth 2024), the physical interpretation of the result is qualitatively similar.

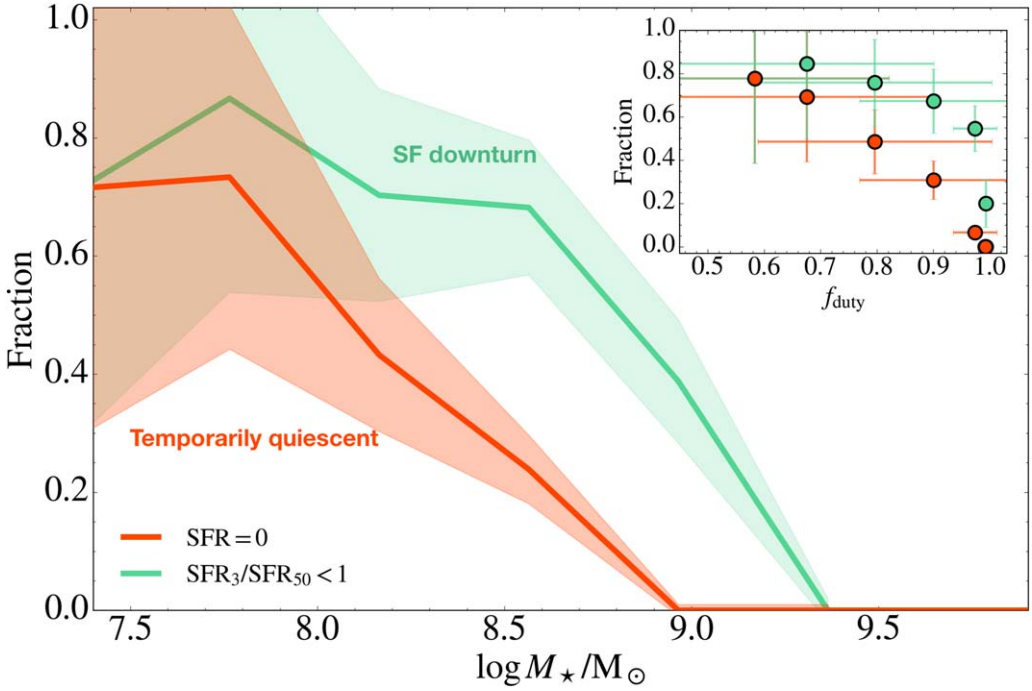

Figure 3. Fraction of SERRA galaxies that are quiescent (SFR = 0) and that are experiencing a downturn in star formation ($SFR_3/SFR_{50} < 1$) galaxies per stellar mass bin. Shown are the 1σ Poisson errors in each bin. The inset shows the same fractions as a function of the average duty cycle in each bin, defined as the fraction of a galaxy's lifetime spent in activity $f_{\rm duty} = \frac{\Delta t(\rm SFR > 0)}{t_{\rm obs} - t_{\rm form}}$, and highlights that lower massive galaxies are more likely quenched and, on average, spend less time in active phase.

by V. Gelli et al. (2023), both satellite and central galaxies undergo similar bursty feedback-regulated evolution, where the quenching is dominated by *internal stellar feedback*. Indeed, V. Gelli et al. (2023) find that SNe feedback is the principal physical mechanism responsible for suppressing star formation in $M_\star < 10^{8.5} M_\odot$ galaxies, typically acting on $\sim$30 Myr timescales (see also A. Pallottini & A. Ferrara 2023, in particular Figure 4 therein). This SN quenching is therefore independent of the environment in which they dwell. The slight difference in the fractions of quiescent galaxies between the two samples is instead related to their ability to resume star formation after being quenched, which can depend on the environment. In particular, we find that satellite galaxies are less likely to replenish their gas reservoirs, as most circumgalactic gas is accreted onto the nearby, more massive galaxy with its deeper gravitational potential. Given the only minor differences between the two classes of galaxies, from now on we will not distinguish between the two and treat the sample of low-mass galaxies all together.

In Figure 2, we also show spectroscopic samples for JWST studies at similar redshifts (S. Fujimoto et al. 2023; K. Nakajima et al. 2023; M. Curti et al. 2024). While the mass range covered by the observations and our simulations is comparable, the observed SFR range predominantly overlaps with the region of the highest star-forming simulated galaxies. Our simulated galaxies are, on average, well aligned with the main sequence parameterization from P. Popesso et al. (2023), but seem to struggle to reach the very-high-SFR regime ($\rm SFR > 50 M_\odot\,yr^{-1}$) covered by most spectroscopic observations. These extreme values occur in the simulation only during short-lived luminous bursts of their SFH ($\lesssim$20 Myr; see A. Pallottini & A. Ferrara 2023), making them statistically less likely to appear in our randomly selected limited sample, but very easy to detect. Conversely, observations of low star-forming galaxies ($\rm SFR \lesssim 1 M_\odot\,yr^{-1}$) or undergoing downturns in star formation($\rm SFR_3/SFR_{50} \lesssim 1 M_\odot\,yr^{-1}$) are rare. This scarcity arises because time variability in the SFR causes fluctuations in galaxy luminosities, making galaxies in phases of declining star formation fainter and thus harder to detect (see Section 4.2). As a result, observations, especially those relying on nebular line selection, are generally biased toward the highly star-forming tail of the galaxy population, and this intrinsic limitation should be carefully considered when inferring galaxy population properties in the EoR.

3.3. Quiescent Fractions

The fraction of galaxies found in a quiescent phase at any given time is expected to be proportional to the overall duration of these periods and inversely proportional to their duty cycle. Therefore, measuring the fraction of temporarily quiescent galaxies is crucial for estimating the duty cycles of high-z galaxies, understanding the timescales of their star formation histories, and gaining insights into the physical processes that regulate them.

We study the mass dependency of the duty cycle of galaxies, by showing in Figure 3 the fraction of quiescent (SFR = 0) and downturn ($\rm SFR_3/SFR_{50} < 1$) galaxies per stellar mass bin. The fractions strongly increase with decreasing stellar mass. For $M_\star > 5 \times 10^8 M_\odot$, quiescent systems represent <10% of the satellite population; at $M_\star \approx 10^{7.5} M_\odot$, the fraction becomes 70%. Similarly, the overall fraction of galaxies with recent SFR downturn follows a decreasing trend with mass, going from $\gtrsim$80% at $M_\star \approx 10^8 M_\odot$ to $\sim$30% at $M_\star \approx 10^9 M_\odot$. The shaded regions show the 1σ Poisson error in each bin, which can reach unphysical values of $\gtrsim$100% in the low-mass regime due to low number counts.

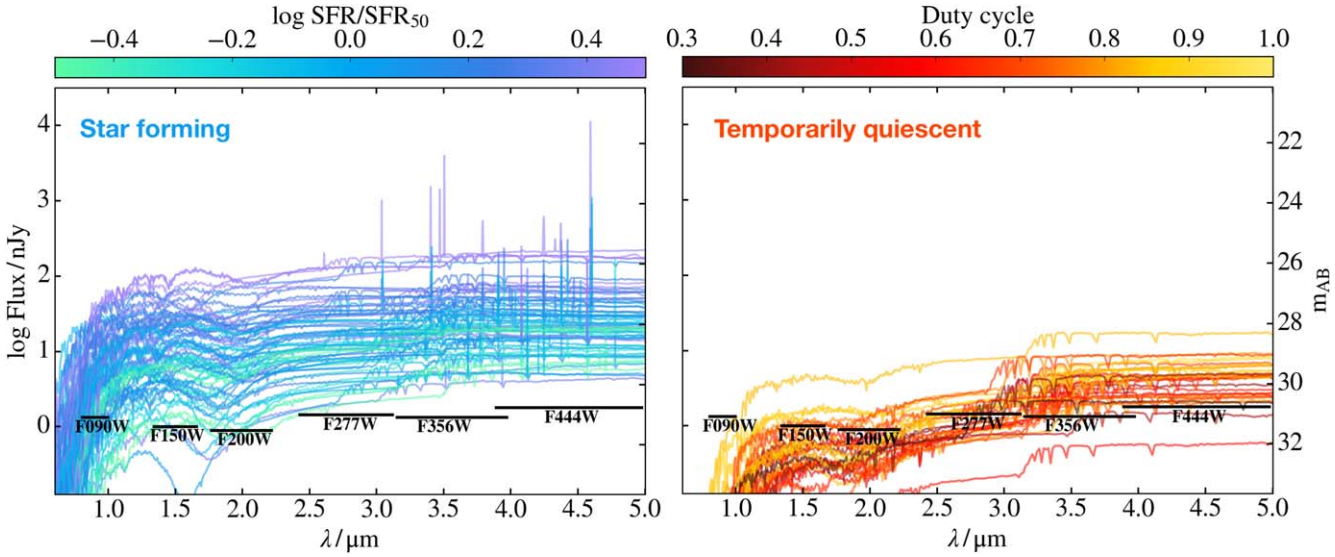

Figure 4. SEDs of the star-forming and temporarily quiescent SERRA galaxies at redshift $6 < z < 8$ in the observed wavelength range covered by JWST/NIRCam and NIRSpec. Horizontal lines are the expected sensitivity limits for NIRCam imaging for a 20 hr exposure observation with S/N ~ 3.

To highlight how these fractions are tightly linked to the bursty nature of the SFH, the inset shows the same fractions as a function of $f_{\rm duty}$ in each bin. At fixed stellar mass, higher fractions of quiescent galaxies reflect lower duty cycles, i.e., less time spent in activity. This strong mass dependency once again reflects the fact that lower-mass systems, typically residing in lower-mass dark matter haloes, are especially sensitive to feedback processes, and their star formation can be more easily suppressed by stellar feedback through SN explosions and photoevaporation of H_2.

Measuring these fractions would provide a direct probe of high-z bursty evolution, but it remains highly challenging for several reasons. First, accurate measurements of stellar mass at high redshift are challenging due to the bursty nature of galaxies' SFH, which are difficult to capture with commonly used SED fitting codes (e.g., V. Markov et al. 2023; L. Whitler et al. 2023; E. Rusta et al. 2024), as well as the outshining of older stellar populations by recent star formation (e.g., D. Narayanan et al. 2024). Second, galaxies undergoing downturns or temporary quiescence are, on average, fainter than their star-forming counterparts of the same mass (see Section 4), making it challenging to achieve the stellar mass completeness required to measure quiescent fractions, particularly at the low-mass end.

For these reasons, for a more reliable comparison between simulations and observations, we will compare fractions of quiescent galaxies at fixed luminosity rather than stellar mass.

In the following sections, we present the results of the forward modeling of the SEDs of SERRA galaxies, allowing us to predict the detectability of temporarily quiescent systems, compare with recent JWST observations, and explore the best observational strategies to better capture this elusive population.

4. Constraining High-z Burstiness with JWST Observations

Having analyzed the bursty evolution of galaxies that leads to the emergence of temporarily quiescent low-mass systems at $z > 6$, we now turn to investigating the impact of this evolution on their emission. In this section, we present the results of forward modeling the galaxies' emission, analyzing the SEDs of both star-forming and quiescent systems, and comparing them with observations.

4.1. Bursty Evolution Shaping the SEDs

In Figure 4, we show the synthetic SEDs of the star-forming (left) and temporarily quiescent (right) galaxies (see Section 2.2 for the model). The flux density is plotted as a function of the observed wavelength in the range $0.6 < \lambda/\mu{\rm m} < 5$, covered by the NIRCam and NIRSpec instruments on board JWST.[11]

The SEDs of star-forming galaxies, which are on average more massive than quiescent ones (Figure 3), are characterized by higher flux at all wavelengths and by the presence of prominent emission lines associated with ongoing star formation. Their SEDs are color coded according to their $\rm SFR_3/SFR_{50}$, highlighting how galaxies undergoing suppressions/downturns in star formation tend to be less luminous and have weaker emission lines than those experiencing bursts. By contrast, spectra of temporarily quiescent galaxies are not only fainter, but they also show strong Balmer breaks produced by the presence of older stellar populations and the lack of young stars contributing to the emission. They are characterized by redder colors, with the emission peaking at $\lambda \gtrsim 3\,\mu$m. Among these temporarily quiescent systems, brighter galaxies are characterized by higher duty cycles, i.e., they have been only recently quenched and have spent the least time in the quiescent phase.

The effect of dust extinction is relevant in some of the star-forming systems with $M_\star \gtrsim 10^{8.5} M_\odot$, where column densities can reach $N_{\rm H} \sim 10^{22}{\rm cm}^{-2}$. Conversely, it is less important in quiescent galaxies where the amount of gas and dust is negligible, having been mostly evacuated or heated by SN explosions.

It is now evident how galaxies experiencing a starbursting phase are more luminous in all filters and easier to detect in large surveys, while only very deep observations can allow for the detection of the less massive quiescent galaxies. Typical NIRCam sensitivity limits for point sources with a signal-to-noise ratio of S/N ~ 3 and an exposure time of $\sim$20 hrs are

[11] The displayed SEDs show the emission without the intergalactic medium absorption, which for galaxies at $z \sim 6$–8 is expected to heavily affect the observed flux in the JWST/NIRCam F090W filter.

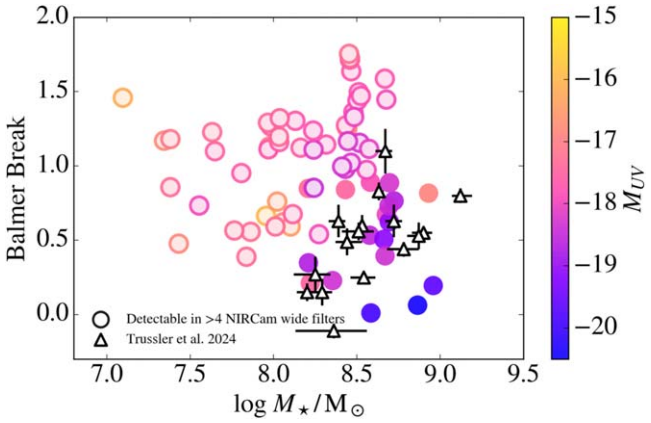

Figure 5. Balmer break strength as a function of the stellar mass for temporarily quiescent galaxies in SERRA. The colors show the UV magnitude, and filled scatter points mark those galaxies that are above typical deep (20 hrs) NIRCam detection limits in at least four wideband filters. Datapoints show observations from temporarily quiescent galaxies in JADES by J. Trussler et al. (2025).

also shown.[12] The fact that many temporarily quiescent galaxies' SEDs are below these values, especially at wavelengths below $\lambda < 3\,\mu$m, highlights how unveiling this population represents a challenge even for the deepest JWST surveys.

4.2. Comparison with JWST Observations

We can now use the synthetic SEDs to translate our predictions for the fractions of temporarily quiescent and downturn galaxies analyzed in Section 3.3 into observable properties. In temporarily quiescent galaxy spectra, a key feature is a strong Balmer break, which strength we can define as the difference between the flux in the filters F277W and F444W.

In Figure 5, we show the strength of the Balmer break as a function of the stellar mass, colored with the UV magnitude. The filled points identify the SERRA galaxies that would be above observational limits for ∼20 hr imaging. We compare with observations from J. Trussler et al. (2025) that identified temporarily quiescent galaxies in JADES from medium and wideband imaging using their lack of emission lines. Interestingly, the observations cover the same Balmer break—$M_\star$ regions as our predicted *detectable* temporarily quiescent galaxies, implying that detected galaxies are indeed sources undergoing drops of star formation due to burstiness. Figure 5 also highlights how temporarily quiescent galaxies with similar stellar mass can exhibit a wide range of luminosities and Balmer breaks, and not all of them exceed the detection limits. For this reason, when comparing fractions of temporarily quiescent galaxies with observations, it is crucial to consider mass incompleteness. To address this issue, we can leverage our forward modeling to explore whether and how the stellar mass dependence of burstiness (see Figure 3) translates into a corresponding luminosity dependence (e.g., G. Sun et al. 2024).

In a recent study, R. Endsley et al. (2024a) analyzed the SFH of over 300 Lyman break galaxies at $z \sim 6$ down to $M_{\rm UV} < -16$, finding a large diversity in $L_{\rm H\alpha}/L_{\rm UV}$, index of recent changes in SFR, among galaxies at the same magnitude. In Figure 6, we compare our predictions for the fractions of bursty galaxies with R. Endsley et al. (2024a) observations. The left panel shows the fractions of galaxies with $\rm SFR_3/SFR_{50} > 1$, i.e., that are experiencing recent bursts of star formation, and those with $\rm SFR_3/SFR_{50} < 0.2$, i.e., that are experiencing extremely strong downturns and that in our sample correspond to temporarily quiescent galaxies. SERRA predicts the fraction of quiescent galaxies to increase for faint galaxies, reflecting the stellar mass dependency (see Figure 3), and to be the dominant (>50%) population above $M_{\rm UV} > -17$. On the other hand, galaxies with a recent increase in star formation are predicted to be more abundant at higher luminosities.

When comparing our predictions to the observations of R. Endsley et al. (2024a), we find that the simulated trends for both types of galaxies align remarkably well with the observed fractions. However, while the increasing abundance of quiescent (starbursting) galaxies toward lower (higher) luminosities is well reproduced, their overall fraction is from 0.01 to 0.15 dex higher in observations compared to the simulation.

The fact that observed "extreme" galaxies, both starbursting and quiescent, are more abundant than the simulations indicates that high-z galaxies have a more bursty evolution than predicted, with shorter duty cycles.

The right panel of Figure 6 shows the cumulative fractions of galaxies in three $M_{\rm UV}$ bins as a function of their burstiness quantified through the ratio $\rm SFR_3/SFR_{50}$. The fractions follow similar general trends, with fainter galaxies being dominated by downturn and quiescent population ($\rm SFR_3/SFR_{50} < 1$), and brighter galaxies exhibit a steeper rise toward higher ratios. The observed trends, especially for the fainter galaxies, rise more slowly than the simulation, hinting once again at the somewhat stronger burstiness encountered in observations, causing higher fractions of galaxies to populate the low $\rm SFR_3/SFR_{50}$ tail at all luminosities.[13]

In Figure 7, we provide further predictions for the fractions of quiescent (SFR = 0) and downturn galaxies ($\rm SFR_3/SFR_{50} < 1$) as a function of the $M_{\rm UV}$ and AB magnitudes in two JWST/NIRCam filters (F150W and F356W, blueward and redward of the Balmer break, respectively). As expected, the fraction of both low star-forming and quiescent galaxies increases toward fainter sources. However, we notice that at fixed $m_{\rm AB}$, the fraction of quiescent galaxies detected in F356W is significantly larger than in F150W. This effect is due to the prominent Balmer break that characterizes these galaxies, making most of them appear only in the redder filters in imaging surveys. In Section 5.2, we explore how this may be exploited to unveil the faintest quiescent galaxies.

5. Discussion

5.1. Interpretation of JWST Observations

We have seen how observations by R. Endsley et al. (2024b) suggest a slightly burstier star formation in observed $z \sim 6$ galaxies than what was predicted in SERRA. Since the evolution

[12] Flux limits for a 10 ks integration are retrieved from Table 1 of https://jwst-docs.stsci.edu/jwst-near-infrared-camera/nircam-performance/nircam-sensitivity (last updated on 2022 November 25th), based on the Exposure Time Calculator v2.0, assuming photometric apertures 2.5 pixels in radius and a benchmark background (1.2 × minimum zodiacal light).

[13] We also note that part of the mismatch is to be attributed to the different overall sample analyzed in simulations and observations: while we selected galaxies with $M_\star < 10^{9.5} M_\odot$ from SERRA, observed galaxies can reach higher masses and luminosities, the reason why the curves do not reach unity in the plot.

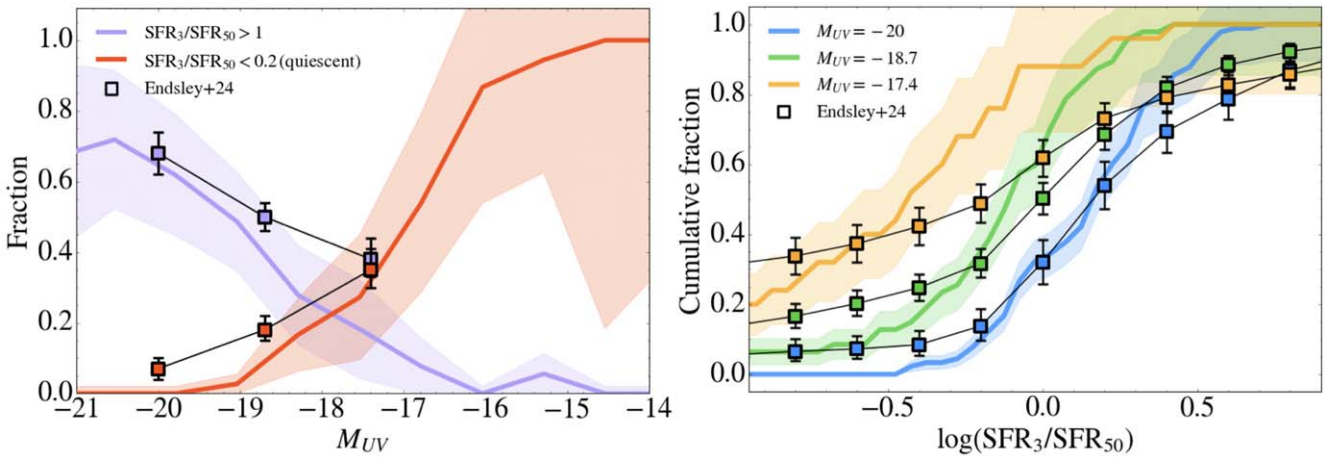

Figure 6. Comparison between SERRA and observations by R. Endsley et al. (2024a). *Left*: fractions of temporarily quiescent galaxies $SFR_3/SFR_{50} < 0.2$ and starburst galaxies $SFR_3/SFR_{50} > 1$ as a function of the UV magnitude. *Right*: cumulative fractions of galaxies in three M_{UV} bins as a function of the SFR ratio. The trends confirm the mass dependence of bursty evolution, with low-mass, fainter galaxies more likely to experience quiescence. The slightly higher observed fraction of bursty galaxies suggests shorter duty cycles and enhanced burstiness in high-z galaxies compared to the simulation.

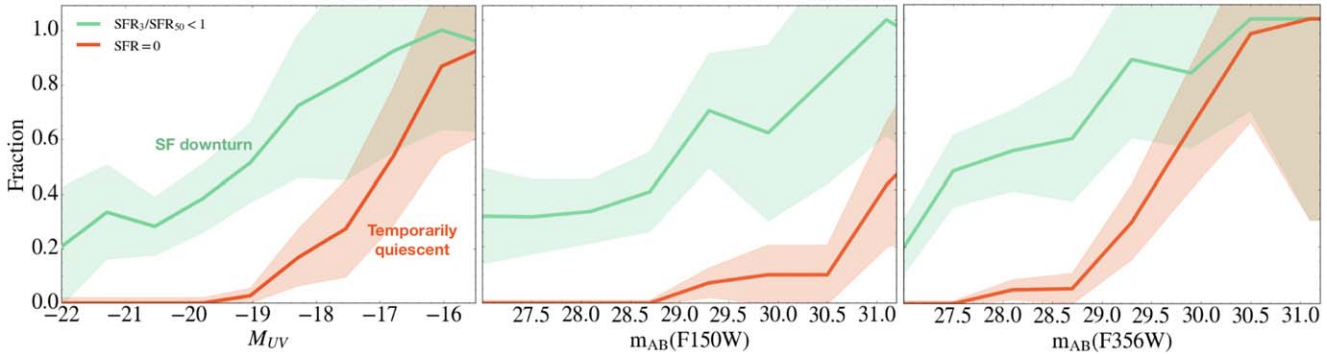

Figure 7. Fractions of temporarily quiescent (red) and downturn (green) galaxies in the SERRA simulations as a function of the absolute magnitude M_{UV} (left panel), and the AB magnitude in two NIRCam filters F150W (central panel) and F356W (right panel), respectively, blueward and redward of the Balmer break.

and quenching of the simulated low-mass galaxies are largely dominated by internal stellar feedback from H_2 photoevaporation and SN explosions, the similar observed trends indicate that these are indeed the main factors driving bursty evolution, but that stronger feedback or additional processes may be at play to boost the burstiness and quenching of galaxies.

One possibility is that the additional required feedback is provided by the action of stronger radiation pressure from young stars (as suggested in A. Ferrara et al. 2023; A. Ferrara 2024) also required to explain the observed spectra of the currently observed quiescent galaxies (V. Strait et al. 2023; T. J. Looser et al. 2024), as shown in V. Gelli et al. (2023), V. Gelli et al. (2024b).

Moreover, R. Endsley et al. (2024b) also report the observation of galaxies undergoing extreme bursts of star formation with $SFR_3/SFR_{50} > 5$, which are not encountered in our sample. This discrepancy is likely primarily due to the stellar mass selection of the galaxies in our sample ($M_\star < 10^{9.5} M_\odot$), but may also partially reflect a higher degree of burstiness in the observed galaxies.

Here, we have focused on galaxies in the final stages of the EoR, as this is the optimal regime where the fluxes of quiescent low-mass systems are high enough to be observed. However, the high level of burstiness inferred is also likely present at very high redshifts $z > 10$, where extreme star formation stochasticity is expected to play a role in enhancing the observed UV luminosities (e.g., C. A. Mason et al. 2023; A. Pallottini & A. Ferrara 2023; V. Gelli et al. 2024a; V. Kokorev et al. 2024).

Our predictions also show how the fractions of temporarily quiescent galaxies are expected to increase even more at lower luminosities, reaching 80% at $M_{UV} \gtrsim -16$. Pushing observations to fainter limits, e.g., with deeper observations or gravitational lensing, would therefore provide crucial insights into the feedback processes regulating bursty star formation. For instance, detecting higher fractions than predicted in this low-luminosity regime would suggest that SN feedback, acting in all galaxies after starbursts, needs to be stronger. Conversely, if the observed trends align with our predictions at $M_{UV} > -16$, it would indicate that the currently observed discrepancy is related to higher-mass galaxies, where different feedback mechanisms, such as AGN, may play a role.

Interestingly, JWST has also been revealing more massive quiescent galaxies at surprisingly high redshifts (e.g., A. C. Carnall et al. 2023; A. de Graaff et al. 2025; V. Kokorev et al. 2024; A. Weibel et al. 2025). Explaining their nature is beyond the scope of this work, as their quiescence is likely not temporary and not linked to bursty star formation, but rather to a stronger feedback mechanism such as AGN feedback. As black hole feedback is not included

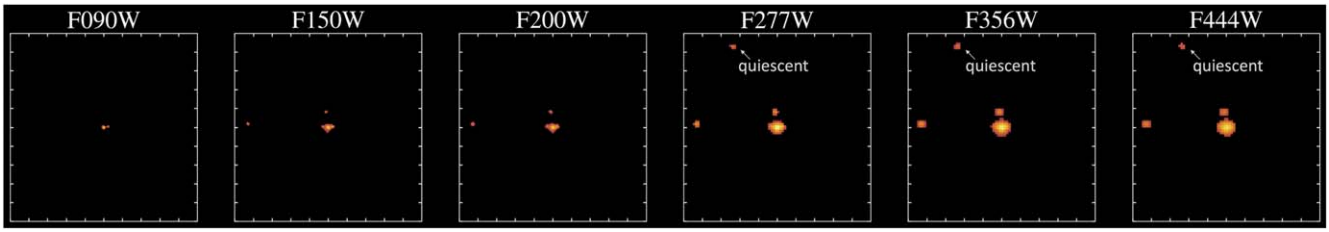

Figure 8. Synthetic image of a group of galaxies at $z \sim 6$ as they would appear in different JWST/NIRCam filters. The colored pixels are those with expected flux at $S/N > 5$ in a typical 20 hr observation. The displayed field of view has a side of 5″ and is centered on a massive ($M_\star \sim 10^{10} M_\odot$) galaxy. One out of its three satellites is a temporarily quiescent F200W dropout galaxy, as pinpointed by the white arrow.

in SERRA, this interpretation would also be consistent with the fact that we do not find any massive quenched galaxy in our sample. In fact, if AGN feedback is indeed at play at $z > 6$, we expect the fractions of quiescent galaxies shown in Figure 3 to increase once again in the high-mass regime, i.e., above $M_\star > 10^{10} M_\odot$.

5.2. Prospects: F200W Dropouts and Satellites

Our predictions show that current observations are typically limited to the more luminous ($M_{\rm UV} < -17$) among the temporarily quiescent galaxies, i.e., the ones that have only been recently quenched. This is expected to be the tip of the iceberg, as our analysis suggests the presence of a large population of hidden quiescent galaxies dominating at lower masses and fainter regimes ($M\star < 10^8 M_\odot$, $M_{\rm UV} > -17$).

To understand whether and how the faintest end of the population of temporarily quenched galaxies may appear in JWST observations, we produce mock NIRCam images for all our simulated systems. In Figure 8, synthetic images of a $z \sim 6$ group of galaxies are shown in different NIRCam filters. Pixels are colored with increasing flux when the signal-to-noise ratio exceeds $S/N > 5$ (black elsewhere), for an exposure time of 20 hrs.

The image, of size 5″ × 5″, corresponding to 30 kpc × 30 kpc, is centered on a massive $M_\star \sim 10^{10} M_\odot$ star-forming galaxy that is surrounded by three lower-mass satellites: two actively star-forming galaxies and one in temporary quiescence. This typical high-z dense environment allows us to understand how different sources may appear in deep JWST imaging surveys. All the low-mass bursty galaxies ($M_\star < 10^{9.5} M_\odot$) appear as compact point sources, while the central, more massive galaxy is more extended and resolved.

The temporarily quiescent galaxy, currently not forming stars and therefore dominated by old stellar populations, appears only in long wavelength filters, as a F200W dropout source. As typical temporarily quiescent SEDs (see Figure 4) are characterized by strong Balmer breaks, the observed flux drops drastically below ∼3 μm, where only upper limits can be placed, even in a ∼20 hr observation. The vast majority of temporarily quiescent galaxies in our sample are predicted to appear as F200W dropouts in typical deep surveys. In particular, mimicking a ∼20 hr exposure, we expect that out of 51 temporarily quenched galaxies, only 25 are bright enough to be observable in at least three NIRCam filters, and 21 of them, i.e., 84%, appear as F200W dropouts. This high fraction suggests that current observations may be overlooking the majority of quiescent galaxies, not identified with current selection methods. Instead, these currently primarily select the brightest among the quiescent galaxies, with emission spanning multiple filters, and whose star formation was only recently suppressed.

Moreover, the predicted fraction of temporarily quiescent sources could be even larger if the star formation is more bursty than expected, as hinted by the results from R. Endsley et al. (2024a) and L. Ciesla et al. (2024). Identifying F200W dropout candidates in deep JWST fields may be the key to exploiting the full potential of current galaxy surveys and uncovering the hidden population of temporarily quiescent galaxies at high redshift.

Relying on photometry of F200W dropout sources to identify temporarily quiescent galaxy candidates is a challenging task given that redshift estimates are inevitably characterized by large uncertainties, up to $\Delta z_{\rm phot} \sim 3$ (see the Appendix, where we test the synthetic photometry with BAGPIPES). However, this issue may be mitigated by exploiting high-z galaxy *overdensities*, like the one shown in the example in Figure 8. We can in fact show that, despite the large photo-z uncertainty, if a quiescent galaxy candidate is found at a close angular distance ($\lesssim$5″) from a massive spectroscopically confirmed galaxy, then the probability of it being a satellite is as high as ∼95% (see the Appendix for details), allowing to confirm its redshift as the same of the host massive galaxy.

As we have seen in Section 3.2, the physical processes driving the quenching of low-mass galaxies are the same for satellite and central dwarf galaxies (i.e., internal feedback processes). However, low-mass quenched galaxies in such dense environments may more likely experience "starvation," as most of the fresh gas from the circumgalactic medium is funneled toward their more massive companions. Consequently, the environment may affect the ability of quenched galaxies to resume star formation and undergo "rejuvenation" (e.g., C. Witten et al. 2025), a scenario we predict to be more likely for central galaxies. Thus, detecting candidates in $z > 6$ galaxy overdensities would allow us to both robustly identify a population of quiescent galaxies and assess potential environmental effects.

6. Summary and Conclusions

Using the SERRA suite of cosmological simulations, we have shown that, as a result of a highly bursty star formation, *temporarily quiescent* low-mass galaxies are expected to be common in the EoR. We built a sample of >200 galaxies ($M_\star < 10^{9.5} M_\odot$), between $6 \lesssim z \lesssim 8$; by analyzing their physical and evolutionary properties, we find that:

1. Bursty star formation leads to a large scatter in the SFR–$M_\star$ relation, increasing toward lower masses, with $\sigma_{\log {\rm SFR}/\langle SFR \rangle} \sim 0.4$ for $M_\star \sim 10^8 M_\odot$.

2. Low-stellar-mass galaxies are easily quenched due to their shallow gravitational potentials, and the fraction of temporarily quiescent galaxies increases with decreasing mass, reaching $\gtrsim$50% of the population for $M_\star < 10^8 M_\odot$.
3. Both *central* and *satellite* galaxies experience temporary quiescence due to internal feedback, indicating that the environment does not play a key role in their quenching. However, the higher fraction of quiescent satellites (32%) compared to centrals (13%) suggests that nearby massive companions may inhibit the efficient re-accretion of fresh gas, favoring starvation (rejuvenation) in satellite (central) galaxies.

We derived the synthetic SEDs of the simulated galaxies, taking both continuum and line emission into account, as attenuated by dust, to compare with JWST observations and make future predictions. The main results are:

1. Temporary quiescent galaxies are typically faint ($\langle M_{\rm UV}\rangle = -15.6$ for $M_\star \sim 10^8 M_\odot$) with a broad range of UV luminosities at fixed stellar mass, and their spectra lack emission lines but exhibit strong Balmer breaks (0–2 for $M_\star \sim 10^{8.5} M_\odot$), consistent with observations by J. Trussler et al. (2025).
2. The fraction of temporarily quiescent (starburst) galaxies rapidly increases (decreases) toward faint luminosities, becoming the dominant population above $M_{\rm UV} > -17$.
3. Predicted fractions for temporarily quiescent galaxies follow similar trends to those observed by R. Endsley et al. (2024a), but are slightly lower (between 1% and 15%) at $-20 < M_{\rm UV} < -19$. The high abundance of extremely starbursting and quiescent galaxies observed means that $z \sim 6$ galaxies undergo an even burstier star formation than in our simulations, suggesting that, on top of the dominant SNe, stronger feedback or additional processes may be at play (e.g., V. Gelli et al. 2023).
4. Most temporarily quiescent galaxies at $z \sim 6$–8 are predicted to be detectable as F200W dropouts in current deep surveys, with galaxy overdensities offering promising environments to locate them as satellites of massive sources, enabling high-confidence photometric identification (95%).

Our results convincingly show that stellar feedback plays a vital role in shaping the SFHs of galaxies during the EoR. Bursty star formation significantly influences the observability of early galaxies over time, introducing a bias in our view of the early Universe toward the more luminous starbursting sources at high redshifts. Accurate predictions of these effects are crucial to be able to effectively interpret observations of galaxy populations at the highest redshifts. JWST has begun to reveal the tip of the iceberg of the vast population of faint, less star-forming galaxies at the edge of reionization. As our models predict these galaxies to be the majority at lower luminosities, upcoming unprecedentedly deep surveys (e.g., GLIMPSE; H. Atek et al. 2023) and specific strategies to target temporary quiescent galaxies will be fundamental to unveil this extremely faint population and expand our knowledge on early galaxy evolution.

Acknowledgments

We thank Ryan Endsley for sharing his data. S.S. acknowledges support by the ERC Starting Grant NEFERTITI H2020/804240 (PI: Salvadori). V.G. and C.A.M. acknowledge support by the Carlsberg Foundation under grant CF22-1322. The Cosmic Dawn Center (DAWN) is funded by the Danish National Research Foundation under grant DNRF140. This work is supported (AF) by the ERC Advanced Grant INTERSTELLAR H2020/740120, and in part by grant NSF PHY-2309135 to the Kavli Institute for Theoretical Physics (KITP). We acknowledge the CINECA award under the ISCRA initiative for the availability of high-performance computing resources and support from the Class B project SERRA HP10BPUZ8F (PI: Pallottini). We gratefully acknowledge the computational resources of the Center for High Performance Computing (CHPC) at SNS. We acknowledge usage of the Python programming language (G. Van Rossum & J. de Boer 1991; G. Van Rossum & F. L. Drake 2009), Astropy (Astropy Collaboration et al. 2013), Cython (S. Behnel et al. 2011), Matplotlib (J. D. Hunter 2007), NumPy (S. van der Walt et al. 2011), PYNBODY(A. Pontzen et al. 2013), and SciPy (P. Virtanen et al. 2020).

Appendix

Based on our results, a promising strategy to find temporarily quiescent galaxies is based on broadband photometry to identify F200W dropout sources. First, we test the expected typical photo-z uncertainties by performing BAGPIPES (A. C. Carnall et al. 2018) SED fitting to mock photometry of our quiescent sources. Figure 9 shows the resulting probability distribution for the redshift of a typical F200W dropout at $z = 7$. The distribution is peaked at the correct redshift but is very broad, leading to large uncertainties of $\Delta z_{\rm phot} \sim 3$.

However, relying on dense environments in close proximity ($<5''$) of spectroscopically confirmed massive galaxies would put stronger constraints on the actual redshift of the F200W dropouts. In fact, confirming that a photodetected source is a satellite of a known massive galaxy would confirm its redshift as the same as the host galaxy's. We need to address the question: what is the probability of a source in the proximity of a massive high-z galaxy to be a satellite galaxy and not a foreground or background interloper?

We can give an answer to this question using a simple probabilistic argument. Given a certain photometric redshift error $\Delta z_{\rm phot}$ compatible with that of a target high-z Lyman break galaxy (LBG), we want to evaluate the probability of a certain source detected in its vicinity (within $<R_{\rm vir}$) to be one of its satellites and not an interloper field galaxy within the same redshift range. This can be quantified as $P({\rm sat}) = \frac{\langle N_{\rm sat}\rangle}{\langle N_{\rm sat}\rangle + N_{\rm field}}$, where $\langle N_{\rm sat}\rangle$ is the average number of expected detectable[14] satellites per LBG system, and $N_{\rm field}$ is the number of expected detectable field galaxies within the same redshift range. To evaluate the latter, we consider the number of galaxies at redshift z in a given magnitude range and cosmic volume V as

$$N_{\rm field} = \int_{M_{\rm min}}^{M_{\rm max}} \phi_z(M)\, dM \times V, \quad (1)$$

where $\phi_z(M)$ is the Schechter luminosity function at redshift z in units mag^{-1} Mpc^{-3} (R. J. Bouwens et al. 2021). As $M_{\rm min}$

[14] We assume a typical deep observation of 20 hr reached in, e.g., JADES, as done in Section 4.

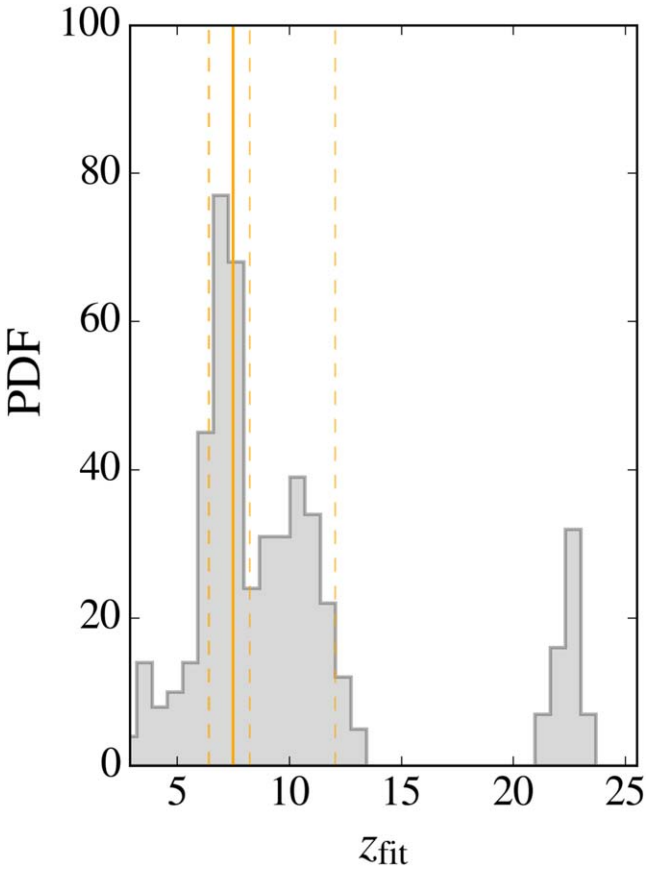

Figure 9. BAGPIPES results for the photometric redshift for a typical temporarily quiescent galaxy.

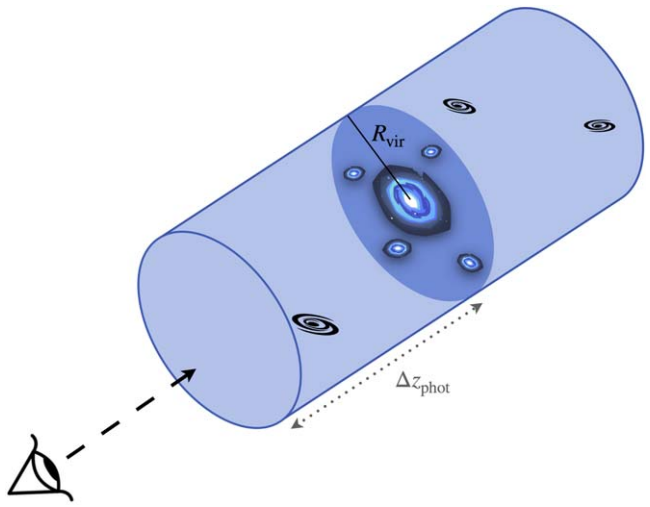

Figure 10. Simple sketch illustrating the possible presence of background or foreground contaminant interloper galaxies (black spiral symbols) in the cosmic volume enclosed by the same redshift range measured for the satellites in the observed region around an LBG.

and $M_{\rm max}$, we consider, respectively, the magnitude of the most luminous of our simulated satellites and the magnitude corresponding to the typical expected sensitivity limit of JWST/NIRCam. The redshift uncertainty enters through the considered cosmic volume V (see the simple illustrative sketch in Figure 10), given by the two-dimensional area of the field of view encompassed within the virial radius, times a depth along the line of sight due to the photometric redshift expected error: $V = \pi R_{\rm vir}^2 (D_L(z + \Delta z_{\rm phot}/2) - D_L(z - \Delta z_{\rm phot}/2))$, where $\Delta z_{\rm phot}$ is taken from our BAGPIPES estimates.

Considering the "worst case scenario" (i.e., maximizing the possible number of interlopers) with: maximum virial radius ($R_{\rm vir} = 25$ kpc), the detectability limit of the deepest JWST surveys in the wide filter F200W at S/N = 3, $\Delta z_{\rm phot}$ as derived by using NIRCam broad bands only, we get $N_{\rm sat} = 2.5$ and $N_{\rm field} = 0.13$. We, therefore, obtain that the probability of a source with a compatible photometric redshift and located near a high-z LBG in the plane of the sky to be a satellite dwarf galaxy is 95%. This confirms that the one proposed is a solid method to identify satellite candidates and infer their properties. Moreover, this argument should be kept in mind, especially when identifying passive dwarf satellites: given their red colors, they could be easily mistaken for higher redshift ($z > 15$) galaxies. Hence, particular attention needs to be paid to such systems located at small angular distances from LBGs.

ORCID iDs

Viola Gelli https://orcid.org/0000-0001-5487-0392
Andrea Pallottini https://orcid.org/0000-0002-7129-5761
Stefania Salvadori https://orcid.org/0000-0001-7298-2478
Andrea Ferrara https://orcid.org/0000-0002-9400-7312
Charlotte Mason https://orcid.org/0000-0002-3407-1785
Stefano Carniani https://orcid.org/0000-0002-6719-380X
Michele Ginolfi https://orcid.org/0000-0002-9122-1700

References

Asada, Y., Sawicki, M., Abraham, R., et al. 2024, MNRAS, 527, 11372
Astropy Collaboration, Robitaille, T. P., Tollerud, E. J., et al. 2013, A&A, 558, A33
Atek, H., Chisholm, J., Alavi, A., et al. 2023, JWST Proposal. Cycle 2, ID. #3293
Baes, M., & Camps, P. 2015, A&C, 12, 33
Baker, W. M., D'Eugenio, F., Maiolino, R., et al. 2025, arXiv:2501.09070
Begley, R., McLure, R. J., Cullen, F., et al. 2025, MNRAS, 537, 3245
Behnel, S., Bradshaw, R., Citro, C., et al. 2011, CSE, 13, 31
Behrens, C., Pallottini, A., Ferrara, A., Gallerani, S., & Vallini, L. 2018, MNRAS, 477, 552
Behroozi, P. S., Wechsler, R. H., & Wu, H.-Y. 2013, ApJ, 762, 109
Bertelli, G., Bressan, A., Chiosi, C., Fagotto, F., & Nasi, E. 1994, A&AS, 106, 275
Bhagwat, A., Costa, T., Ciardi, B., Pakmor, R., & Garaldi, E. 2024, MNRAS, 531, 3406
Bouwens, R. J., Oesch, P. A., Stefanon, M., et al. 2021, AJ, 162, 47
Bouwens, R. J., Smit, R., Schouws, S., et al. 2022, ApJ, 931, 160
Carnall, A. C., McLure, R. J., Dunlop, J. S., & Davé, R. 2018, MNRAS, 480, 4379
Carnall, A. C., McLure, R. J., Dunlop, J. S., et al. 2023, Natur, 619, 716
Chaves-Montero, J., & Hearin, A. 2021, MNRAS, 506, 2373
Ciesla, L., Elbaz, D., Ilbert, O., et al. 2024, A&A, 686, A128
Cole, J. W., Papovich, C., Finkelstein, S. L., et al. 2025, ApJ, 979, 193
Curti, M., Maiolino, R., Curtis-Lake, E., et al. 2024, A&A, 684, A75
de Graaff, A., Setton, D. J., Brammer, G., et al. 2025, NatAs, 9, 280
Dome, T., Tacchella, S., Fialkov, A., et al. 2024, MNRAS, 527, 2139
Endsley, R., Chisholm, J., Stark, D. P., Topping, M. W., & Whitler, L. 2024a, arXiv:2410.01905
Endsley, R., Stark, D. P., Whitler, L., et al. 2024b, MNRAS, 533, 1111
Faisst, A. L., & Morishita, T. 2024, ApJ, 971, 47
Ferland, G. J., Chatzikos, M., Guzmán, F., et al. 2017, RMxAA, 53, 385
Ferrara, A. 2024, A&A, 684, A207
Ferrara, A., Pallottini, A., & Dayal, P. 2023, MNRAS, 522, 3986
Ferrara, A., Sommovigo, L., Dayal, P., et al. 2022, MNRAS, 512, 58
Fujimoto, S., Arrabal Haro, P., Dickinson, M., et al. 2023, ApJL, 949, L25
Furlanetto, S. R., & Mirocha, J. 2022, MNRAS, 511, 3895
Gelli, V., Mason, C., & Hayward, C. C. 2024a, ApJ, 975, 192
Gelli, V., Salvadori, S., Ferrara, A., & Pallottini, A. 2024b, ApJ, 964, 76

Gelli, V., Salvadori, S., Ferrara, A., Pallottini, A., & Carniani, S. 2021, ApJL, 913, L25
Gelli, V., Salvadori, S., Ferrara, A., Pallottini, A., & Carniani, S. 2023, ApJL, 954, L11
Gelli, V., Salvadori, S., Pallottini, A., & Ferrara, A. 2020, MNRAS, 498, 4134
Giménez-Arteaga, C., Fujimoto, S., Valentino, F., et al. 2024, A&A, 686, A63
Grassi, T., Bovino, S., Schleicher, D. R. G., et al. 2014, MNRAS, 439, 2386
Hahn, O., & Abel, T. 2011, MNRAS, 415, 2101
Heintz, K. E., Brammer, G. B., Giménez-Arteaga, C., et al. 2023, NatAs, 7, 1517
Hunter, J. D. 2007, CSE, 9, 90
Iyer, K. G., Speagle, J. S., Caplar, N., et al. 2024, ApJ, 961, 53
Iyer, K. G., Tacchella, S., Genel, S., et al. 2020, MNRAS, 498, 430
Katz, H., Kimm, T., Ellis, R. S., Devriendt, J., & Slyz, A. 2023, MNRAS, 524, 351
Kennicutt, R. C., Jr. 1998, ApJ, 498, 541
Knollmann, S. R., & Knebe, A. 2009, ApJS, 182, 608
Kohandel, M., Pallottini, A., Ferrara, A., et al. 2020, MNRAS, 499, 1250
Kokorev, V., Chisholm, J., Endsley, R., et al. 2024, ApJ, 975, 178
Kravtsov, A., & Belokurov, V. 2024, arXiv:2405.04578
Kroupa, P. 2001, MNRAS, 322, 231
Langeroodi, D., & Hjorth, J. 2024, arXiv:2404.13045
Laporte, N., Ellis, R. S., Boone, F., et al. 2017, ApJL, 837, L21
Leitherer, C., Schaerer, D., Goldader, J. D., et al. 1999, ApJS, 123, 3
Leja, J., Carnall, A. C., Johnson, B. D., Conroy, C., & Speagle, J. S. 2019, ApJ, 876, 3
Looser, T. J., D'Eugenio, F., Maiolino, R., et al. 2023, arXiv:2306.02470
Looser, T. J., D'Eugenio, F., Maiolino, R., et al. 2024, Natur, 629, 53
Ma, X., Hopkins, P. F., Garrison-Kimmel, S., et al. 2018, MNRAS, 478, 1694
Markov, V., Gallerani, S., Pallottini, A., et al. 2023, A&A, 679, A12
Mason, C. A., Trenti, M., & Treu, T. 2023, MNRAS, 521, 497
Mirocha, J., & Furlanetto, S. R. 2023, MNRAS, 519, 843
Morishita, T., Stiavelli, M., Grillo, C., et al. 2024, ApJ, 971, 43
Nakajima, K., Ouchi, M., Isobe, Y., et al. 2023, ApJS, 269, 33
Narayanan, D., Lower, S., Torrey, P., et al. 2024, ApJ, 961, 73
Navarro-Carrera, R., Rinaldi, P., Caputi, K. I., et al. 2024, arXiv:2410.23249
Nikolić, I., Mesinger, A., Davies, J. E., & Prelogović, D. 2024, A&A, 692, A142
Pallottini, A., & Ferrara, A. 2023, A&A, 677, L4
Pallottini, A., Ferrara, A., Bovino, S., et al. 2017a, MNRAS, 471, 4128
Pallottini, A., Ferrara, A., Decataldo, D., et al. 2019, MNRAS, 487, 1689
Pallottini, A., Ferrara, A., Gallerani, S., Salvadori, S., & D'Odorico, V. 2014, MNRAS, 440, 2498
Pallottini, A., Ferrara, A., Gallerani, S., et al. 2017b, MNRAS, 465, 2540
Pallottini, A., Ferrara, A., Gallerani, S., et al. 2022, MNRAS, 513, 5621
Pallottini, A., Ferrara, A., Gallerani, S., et al. 2024, arXiv:2408.00061
Planck Collaboration, Ade, P. A. R., Aghanim, N., et al. 2014, A&A, 571, A16
Pontzen, A., Rovskar, R., Stinson, G. S., et al., 2013 pynbody: Astrophysics Simulation Analysis for Python, Astrophysics Source Code Library, ascl:1305.002
Popesso, P., Concas, A., Cresci, G., et al. 2023, MNRAS, 519, 1526
Prieto-Lyon, G., Strait, V., Mason, C. A., et al. 2023, A&A, 672, A186
Rosdahl, J., Blaizot, J., Aubert, D., Stranex, T., & Teyssier, R. 2013, MNRAS, 436, 2188
Rusta, E., Salvadori, S., Gelli, V., Koutsouridou, I., & Marconi, A. 2024, ApJL, 974, L35
Schmidt, M. 1959, ApJ, 129, 243
Shen, X., Vogelsberger, M., Boylan-Kolchin, M., Tacchella, S., & Kannan, R. 2023, MNRAS, 525, 3254
Strait, V., Brammer, G., Muzzin, A., et al. 2023, ApJL, 949, L23
Sun, G., Faucher-Giguère, C.-A., Hayward, C. C., & Shen, X. 2023a, MNRAS, 526, 2665
Sun, G., Faucher-Giguère, C.-A., Hayward, C. C., et al. 2023b, ApJL, 955, L35
Sun, G., Muñoz, J. B., Mirocha, J., & Faucher-Giguère, C.-A. 2024, JCAP, 2025, 034
Tacchella, S., Forbes, J. C., & Caplar, N. 2020, MNRAS, 497, 698
Teyssier, R. 2002, A&A, 385, 337
Topping, M. W., Stark, D. P., Endsley, R., et al. 2022, ApJ, 941, 153
Trussler, J., Conselice, C., Adams, N., et al. 2025, MNRAS, 537, 3662
Vallini, L., Pallottini, A., Ferrara, A., et al. 2018, MNRAS, 473, 271
van der Walt, S., Colbert, S. C., & Varoquaux, G. 2011, CSE, 13, 22
Van Rossum, G., & de Boer, J. 1991, CWI Quarterly, 4, 283
Van Rossum, G., & Drake, F. L. 2009, Python 3 Reference Manual (Scotts Valley, CA: CreateSpace)
Virtanen, P., Gommers, R., Oliphant, T. E., et al. 2020, NatMe, 17, 261
Weibel, A., de Graaff, A., Setton, D. J., et al. 2025, ApJ, 983, 11
Weingartner, J. C., & Draine, B. T. 2001, ApJ, 548, 296
Whitler, L., Stark, D. P., Endsley, R., et al. 2023, MNRAS, 519, 5859
Wise, J. H., Abel, T., Turk, M. J., Norman, M. L., & Smith, B. D. 2012, MNRAS, 427, 311
Witten, C., McClymont, W., Laporte, N., et al. 2025, MNRAS, 537, 112